DOI: 10.1002/ejic.200601173

Structural Chemistry of a New 10H Hexagonal Perovskite: $BaMn_{0.4}Fe_{0.6}O_{2.73}$

Laura Miranda,[a] Julio Ramírez-Castellanos,[a] María Hernando,[a,b] Aurea Varela,[a] José M. González-Calbet,[a] and Marina Parras*[a]

Keywords: Hexagonal perovskites / Magnetic properties / Mn polytypes / High-resolution electron microscopy

A new 10H polytype has been stabilized in the $BaMn_{1-x}Fe_xO_{3-y}$ system with the composition $BaMn_{0.4}Fe_{0.6}O_{2.73}$. The anionic composition has been established by a reduction and re-oxidation cycle in the stability range of this phase. The structural characterization was carried out by high-resolution electron microscopy (HREM), electron diffraction, and X-ray diffraction. The structure is closely related to the ideal $(hch'ch)_2$ 10H polytype with two oxygen-deficient hexagonal (h′) BaO_{2-y} layers per unit formula. This framework gives rise to blocks of three octahedra sharing faces linked by corners to two corner-sharing tetrahedra.

Introduction

The perovskite family is one of the series of oxides most widely studied in the field of solid state chemistry. The compositional flexibility of a perovskite is reflected in the ability of its structure to accommodate a large variety of cations into the oxygen framework due, in part, to the huge range of structurally related polymorphs which can be adopted. The crystal structures of perovskites, ABO_3, can be considered to consist of stacks of pseudo-close-packed layers AO_3; the smaller B cations occupy the oxygen octahedral holes between the layers. When all the AO_3 layers stack in a cubic close-packed structure (ABC sequence), the $[BO_6]$ octahedra form the three-dimensional, corner-sharing network of the well-known cubic perovskite of the 3C structural type. On the contrary, if all the AO_3 layers are in a hexagonal close-packing structure (AB sequence), the octahedra sharing faces and the one-dimensional 2H structural type (hexagonal perovskite) is obtained. In general, the hexagonal perovskites are less common than the cubic ones because of unfavorable electrostatic cation repulsion associated with the much shorter B–B distance between adjacent face-sharing octahedra.

Between hexagonal and cubic perovskites, a wide range of hexagonal polytypes has been described, whose structures arise from different cubic (c) and hexagonal (h) periodic mixed sequences of the AO_3 layers. These polytypes are usually referred to by the symbols nH or nR, where n corresponds to the number of layers per unit cell, while H and R denote the hexagonal and rhombohedral symmetry, respectively, of the corresponding unit cell.

Many compounds with a hexagonal perovskite-type structure have been reported during the last years. The cation size, the electronic configuration of the B cations, and the oxygen stoichiometry are factors that strongly influence the stabilization of a particular polytype for a given composition. $BaMnO_3$[1] crystallizes in the 2H hexagonal type (**…**hhh**…** sequence). In this system, the introduction of anionic vacancies leads to the stabilization of a large number of anion-deficient $BaMnO_{3-y}$ hexagonal polytypes containing 100–50% hexagonal stacking.[2–5] This behavior is also observed in the $BaFeO_{3-y}$ system, which has been extensively studied in the $0 < y \leq 0.5$ compositional range.[6–10] This system is characterized by a large structural variety; in particular, three different hexagonal polytypes are stabilized for the more oxidized samples. Unlike in the Ba-Mn-O system, stoichiometric $BaFeO_3$ has not been stabilized up to now, but the closest anionic composition, $BaFeO_{2.95}$, adopts the 6H hexagonal polytype with a $(hcc)_2$ stacking arrangement containing only 33% hexagonal layers,[11] that is, much less than $BaMnO_3$. This feature can be related to the bigger size of Fe^{IV} relative to that of Mn^{IV}, both of which are in an octahedral oxygen environment (r_{Fe}^{IV} = 0.585 Å, r_{Mn}^{IV} = 0.550 Å).[12] Actually, in general, an increase of the cubic layers per unit cell occurs when the r_A/r_B ratio decreases, because of the increase of the cationic repulsion in the face-sharing octahedra.

Similarly, different structural modifications have been reported within more complex systems where two or more cations of different chemical nature occupy the B position of the perovskite. Taking into account the great number of polytypes that can be stabilized in the above-mentioned Ba-Mn-O and Ba-Fe-O systems, a diverse structural chemistry may be expected for the $BaMn_{1-x}Fe_xO_{3-y}$ system. This fact,

[a] Dpto. de Química Inorgánica, Facultad de Químicas, Universidad Complutense de Madrid,
28040 Madrid, Spain
Fax: +34-91-394-43-52
E-mail: mparras@quim.ucm.es
[b] Institut Laue Langevin
BP 156X, 38042 Grenoble, France

besides the current interest in the physical properties of Mn-containing perovskites, provides a significant motivation for investigating the effects of substituting Fe for Mn in $BaMnO_3$. Previous work in $BaMn_{1-x}Fe_xO_{3-y}$ involved the stabilization of a 6H polytype (hhhchc sequence) for the $0 \leq x \leq 0.3$ compositional range.[13] All the samples are oxygen-deficient. In view of the sensitivity of the structural chemistry to cation size or redox chemistry, it seems reasonable that changes in the cationic distribution of the B sites are accompanied by structural changes. Therefore, we have investigated this system and we have identified a new single phase adopting a 10H hexagonal polytype. We report in this paper the synthesis and the structural study, of $BaMn_{0.4}Fe_{0.6}O_{3-y}$, carried out by using X-ray diffraction, selected area electron diffraction (SAED), and high-resolution electron microscopy (HREM).

Results and Discussion

Microstructural Characterization

The initial characterization of $BaMn_{0.4}Fe_{0.6}O_{3-y}$ by X-ray diffraction suggests that it is a hexagonal single-phase material with unit cell dimensions corresponding to a 10H polytype. There are twelve stacking sequences of the BaO_3 layers which can result in a 10H cell. Three of them correspond to a $P6_3/mmc$ space group whereas the other nine correspond to space groups without systematic extinctions ($P\bar{6}m2$, $P\bar{3}m1$ and $P3m1$).

The SAED patterns along the most relevant zone axes [001], [010], and [1$\bar{1}$0], are shown in Figure 1a, b, and c, respectively. The diffraction spots are always sharp, and no streaking or diffuse intensity is observed. All the reflections appearing in these patterns can be indexed on the basis of a hexagonal unit cell of lattice parameters close to a = 5.7, c = 24.7 Å. In addition, as it can be observed in the SAED pattern in Figure 1b, the reflection conditions are compatible with a $P6_3/mmc$ space group. By tilting 30° around the c^* axis (Figure 1c), all the spots due to multiple diffraction are visible. According to these results, three stacking sequences are possible for this 10H structure: $(ccccch)_2$, $(hhhcc)_2$, and $(hchch)_2$. The first one presents a much greater proportion of cubic layers than the other two; this sequence has been found in $SrMn_{0.7}Fe_{0.3}O_{2.87}$.[14] The bigger size of the barium atom allows the stabilization of polytypes with a large component of hexagonal perovskite; therefore, one of the other two sequences (containing a 60% of hexagonal layers) seems to be more probable.

Electron microscopy is a very efficient tool for determining the layer-stacking sequence along the c axis. Figure 2a corresponds to the HREM along the [010] axis. In this zone, the structure is viewed parallel to the columns of close-packed Ba–O rows, and therefore the sequence of the layers is directly revealed. In fact, in the hexagonal polytypes, the image contrast along the [010] projection consists of lines of dots in which the straight segments correspond to adjacent cubic (c) layers, whereas every change of slope is associated to the presence of hexagonal (h) layers. Ac-

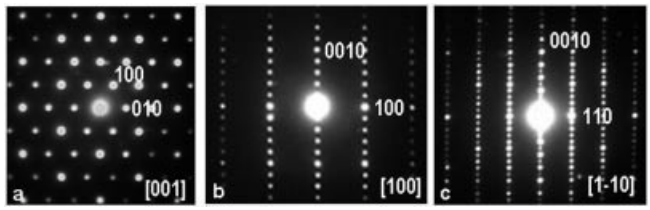

Figure 1. SAED patterns corresponding to $BaMn_{0.4}Fe_{0.6}O_{2.73}$ along (a) [001], (b) [010] and (c) [1$\bar{1}$0].

cording to this, the observed contrast of the image (see Figure 2b) can be interpreted as corresponding to a $(hchch)_2$ layer arrangement. Therefore, from the ideal atomic coordinates corresponding to this 10H sequence, an image calculation was performed. The simulated image (inset of Figure 2a) nicely fits the experimental one for Δt = 70 Å, Δf = –500 Å. This result shows that $BaMn_{0.6}Fe_{0.4}O_{3-y}$ either actually exhibits this hexagonal 10H structure or has a closely related structural type. In this structure (Figure 3a), blocks of three face-sharing octahedra are linked by their terminal corners to blocks of two face-sharing octahedra. It is worth mentioning that this hexagonal polytype is stable in both the Ba-Mn-O and the Ba-Fe-O systems for the compositions $BaMnO_{2.90}$[2] and $BaFeO_{2.80}$,[9,10] respectively.

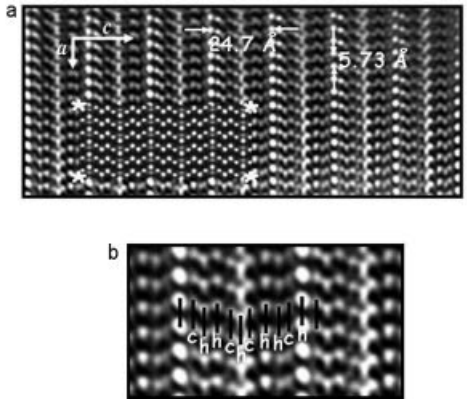

Figure 2. (a) HRTEM image of $BaMn_{0.4}Fe_{0.6}O_{2.73}$ along [010]; the calculated image is shown in the inset. (Δt = 70 Å, Δf = –500 Å) (b) Enlarged image showing the stacking sequence of the BaO_3 layers along the c axis.

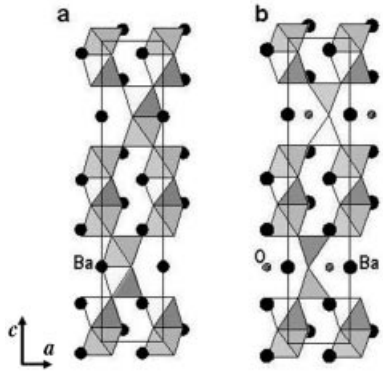

Figure 3. Structural models corresponding to: (a) the 10H-ABO_3 polytype; (b) 10H-$BaFeO_{2.80}$ (according to ref.[10]). Only the Ba and nonbonding O atoms are marked.

Compositional Characterization

The cationic composition was determined by energy-dispersive X-ray spectroscopy (EDS). In order to ensure the chemical homogeneity of the sample, the analysis was performed not only on several dozens of crystallites, but also in different crystal zones. Initially, the absence of Al (from crucible material) in the crystals was confirmed by a preliminary search of all the elements present in the studied samples. Once the lack of additional elements was confirmed, the Ba/Mn/Fe ratio was obtained from the relative intensity of the Ba-$L_\alpha 1$ (4.466 eV), Mn-$K_\alpha 1$ (5.899 eV), and Fe-$K_\alpha 1$ (6.404 eV) lines in the EDS spectra. The obtained result, $Ba_{1.00(2)}Mn_{0.39(3)}Fe_{0.61(1)}O_x$, is in agreement with the nominal composition.

The sample is rather insoluble and we were unable to perform a volumetric analysis to determine the oxygen content. Therefore, in order to establish the anionic stoichiometry, we have undertaken a thermogravimetric study of the sample. First, the sample was reduced under a 300-mbar H_2/200-mbar He atmosphere and heated at 3 °C/min up to 700 °C (Figure 4). Under these experimental conditions, the weight loss is close to 7.1%, BaO, MnO, FeO, and Fe metal being identified by XRD as final products of the reduction. However, since the FeO/Fe ratio in the final products is not known, it is not possible to obtain the oxygen content of the studied sample from this experiment. Unfortunately, even for the most reductive conditions, a FeO/Fe mixture was always obtained. Therefore, in order to estimate the oxygen content, it was necessary to design a different reduction pathway.

In this context, the oxygen content of the above sample can be obtained by thermogravimetric analysis if its anionic compositional range is known. In fact, $BaFeO_{2.80}$[9] adopts the same 10H structural type as the anionic vacancies located in the hexagonal layers on the dimer structural units, changing its anionic composition from BaO_3 to BaO_2 (Figure 3b). The remaining two oxygen atoms rearrange in such a way that only one of them is bonded to the two Fe atoms adjacent to the layer, thus leading to a dimer of corner-sharing tetrahedra. The other oxygen is a nonbonding atom. For lower oxygen content, this nonbonding oxygen is partially removed, and this results in a hexagonal BaO_{2-y} layer.[10] On the basis of the crystallochemical analysis of this phase, we propose that, in a similar way, the anionic range of the stability of the 10H-$BaMn_{0.4}Fe_{0.6}O_{3-y}$ phase varies from 2.80 to 2.60, which corresponds to the range from an h-BaO_2 down to an h-BaO layer from one to zero nonbonding oxygen atoms, respectively. According to this assumption, the anionic composition of $BaMn_{0.4}Fe_{0.6}O_{3-y}$ can be obtained from a reduction and re-oxidation cycle of the sample.

Let us go back now to the reduction curve in Figure 4. In inset (a), a slight change in the slope is visible at 375 °C, corresponding to a weight loss close to 0.9%, that could indicate the existence of a stable phase with lower oxygen content. Therefore, in order to stabilize this reduced phase, we have carried out a partial reduction of the starting material under a 100-mbar H_2/400-mbar He atmosphere by heating at 2 °C/min up to 280 °C for 12 h to ensure oxygen homogeneity in the final product. This reduction process is represented in Figure 5. The lost weight between the starting and the final points amounts to 0.88%. In addition, the X-ray data shows that the reduced phase maintains the basic structural features of the 10H phase. Taking into account the above considerations, if we assume that the stabilized phase corresponds to the lowest limit of the 10H anionic stability range, i.e., $BaMn_{0.4}Fe_{0.6}O_{2.60}$, $BaMn_{0.4}Fe_{0.6}O_{2.73}$ should be the composition of the starting material.

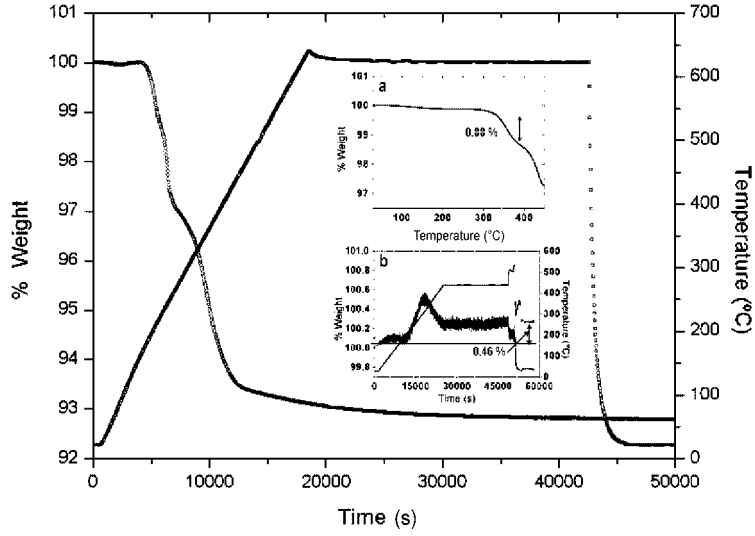

Figure 4. Thermogravimetric analysis of $BaMn_{0.4}Fe_{0.6}O_{3-y}$. The experiment was carried out in a 300-mbar H_2/200-mbar He atmosphere. Inset (a): The temperature dependence of the weight loss. Inset (b): Thermogravimetric curve corresponding to the oxidation of $BaMn_{0.4}Fe_{0.6}O_{3-y}$.

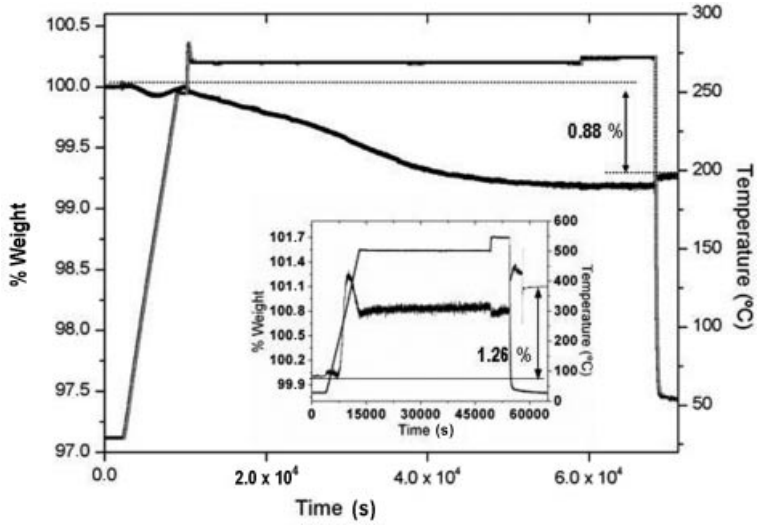

Figure 5. Thermogravimetric curve corresponding to the reduction process (100-mbar H_2/400-mbar He; 2 °C/min up to 270 °C) from the starting material, $BaMn_{0.4}Fe_{0.6}O_{3-y}$, up to a composition of $BaMn_{0.4}Fe_{0.6}O_{2.60}$. The re-oxidation process is shown in the inset.

On the other hand, the starting material was also heated at 2 °C/min up to 400 °C under 1 atm O_2 in a CAHN electrobalance. As shown in inset (b) of Figure 4, the weight of the sample increases slightly with temperature up to a gain of 0.46%. The low stability of the equipment (CAHN electrobalance) used for data collection when working at a static gas pressure of 1 atm gives rise to high data dispersion, which is reflected in the thickness of the oxidation line. However, this experimental aspect does not influence the reliability of the determined oxygen content since both initial and final weight are measured at 0.5-mbar He in a static atmosphere. The XRD pattern of the final product shows that the oxidized sample also maintains the 10H structure of the starting phase. Taking into account the above considerations, this process should be associated to the oxidation from the starting material up to the most oxidized 10H sample, i.e., according to previous results, to the reaction: $BaMn_{0.4}Fe_{0.6}O_{2.73} + O_2 \rightarrow BaMn_{0.4}Fe_{0.6}O_{2.80}$. For this process, the theoretical weight gain corresponds to 0.47%, which nicely fits with the experimental one of 0.46%.

Finally, we have completed this cycle by the re-oxidation of the reduced $BaMn_{0.4}Fe_{0.6}O_{2.60}$ sample (see inset of Figure 5). In this process, the sample weight increases up to 1.26%, in agreement with the $BaMn_{0.4}Fe_{0.6}O_{2.60} + O_2 \rightarrow BaMn_{0.4}Fe_{0.6}O_{2.80}$ reaction (theoretical value: 1.36%). This result supports the previous ones; therefore, from this thermogravimetric study, the anionic stoichiometry of the studied sample is $BaMn_{0.4}Fe_{0.6}O_{2.73}$.

Structural Refinement

According to the above results, $BaMn_{0.4}Fe_{0.6}O_{2.73}$ adopts a structure based on a 10H-$(hch'ch)_2$ sequence. A structural study by X-ray profile refinement has been performed by taking as starting model the structural parameters of the hexagonal 10H-$BaFeO_{2.80-y}$ in the space group $P6_3/mmc$.[9]

Because of their similar scattering factors, Mn and Fe are indistinguishable by XRD; therefore, both metals were randomly distributed over the two crystallographically different octahedral sites, the tetrahedral one is fully occupied by Fe, since neither Mn^{III} nor Mn^{IV} are stable in this oxygen coordination. In addition, the determined anionic stoichiometry indicates the presence of oxygen vacancies in the structure, which, according to the above considerations, have been located into the hexagonal h′-BaO_2 up to a $BaO_{1.65}$ anionic composition; the nonbonding oxygen position (2c) being 65% occupied. This structural feature will be confirmed by neutron diffraction.

The refinement was stable, and it was possible to refine the positions of the oxygen atoms and the isotropic temperature factor for each type of atom (Ba, Mn/Fe, O). Figure 6 shows the graphical results of the fitting of the experimental X-ray diffraction pattern and the difference between observed and calculated data. The final structural parameters are given in Table 1; Table 2 shows selected interatomic distances.

A schematic representation of the structure is depicted in Figure 7. The octahedron at the center of the trimer, M_3O_6, is regular with six identical M–O bonds of length 1.918 Å. This value is in excellent agreement with Mn–O bond lengths observed for Mn^{IV} in the same environment as 2H-$BaMnO_3$ (1.9044 Å),[15] and it is also close to that found in 10H-$BaFeO_{2.8-y}$ for Fe^{III} in octahedral coordination ($d_{average}$ = 2.01 Å).[9,10] In contrast, the $M1O_6$ octahedron is quite distorted, with three long and three short M–O bonds (see Table 2), indicating that metals in this position are displaced from the center toward the oxygen atoms in the cubic layer (O1), i.e., to the neighboring tetrahedra sharing a corner, and hence away from the shared face. As a consequence, with respect to the ideal structure, the M3···M1 distance increases, reducing the electrostatic repulsion between cations in adjacent face-sharing polyhedra. This feature is shown by other polytypes with structural

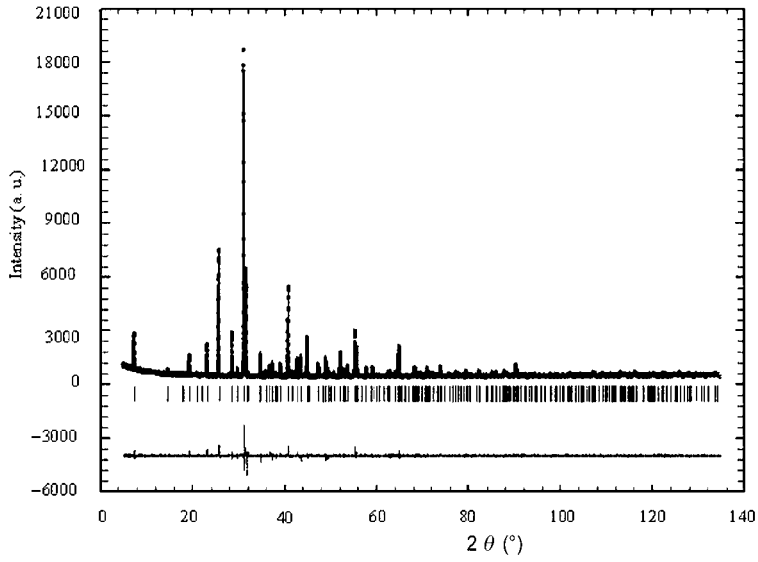

Figure 6. Experimental, calculated, and difference X-ray diffraction patterns corresponding to $BaMn_{0.4}Fe_{0.6}O_{2.73}$.

Table 1. Final structural parameters of $BaMn_{0.4}Fe_{0.6}O_{2.73}$.[a]

Atom	Site	*x*/*a*	*y*/*b*	*z*/*c*	B_{iso}(Å^2)	Occ.
Ba1	2*b*	0	0	0.25	0.47(3)	1
Ba2	4*f*	1/3	2/3	0.36627(6)	0.47(3)	1
Ba3	4*f*	1/3	2/3	0.95936(7)	0.47(3)	1
M1	4*e*	0	0	0.60771(1)	0.94(6)	1
Fe2	4*f*	1/3	2/3	0.82148(2)	0.94(6)	1
M3	2*a*	0	0	0	0.94(6)	1
O1	12*k*	0.319(2)	0.1596(8)	0.3501(3)	1.1(1)	1
O2	12*k*	0.696(1)	0.8479(8)	0.4510(3)	1.1(1)	1
O3	2*d*	1/3	2/3	0.75	1.1(1)	1
O4	2*c*	1/3	2/3	0.25	1.1(1)	0.648[b]

[a] Space group: $P6_3/mmc$ a = 5.74644(4) Å, c = 24.0433(2); R_B = 6.81, R_{exp} = 4.31, R_{wp} = 5.82, χ^2 = 1.82; M = Mn and Fe cations. [b] The O4 occupancy factor has been fixed.

Table 2. Selected interatomic distances (Å) in $BaMn_{0.4}Fe_{0.6}O_{2.73}$.

Ba1–O1 2.883(7) × 6	M1–O1 1.886(5) × 3
Ba1–O3 3.318(3) × 3	M1–O2 2.069(6) × 3
Ba1–O4 3.318(3) × 3	
	M2–O1 1.860(5) × 3
	M2–O3 1.718(4)
Ba2–O1 2.900(6) × 6	M2–O4 3.672(1)
Ba2–O2 2.721(6) × 3	
Ba2–O4 2.796(1)	M3–O2 1.918(6) × 6
Ba3–O1 3.146(6) × 3	M1–M2 3.729(2)
Ba3–O2 2.883(6) × 6	M1–M3 2.589(4)
Ba3–O2 2.811(6) × 3	M2–M2 3.437(1)

octahedral trimers like 9R-$BaIr_xMn_{1-x}O_3$.[16] In addition, these M–O octahedral bond lengths [$d_{average}(M2O_6)$ = 1.97 Å] agree with those of the Ba-Mn/Fe-O polytypes, for instance, in 6H-$BaMn_{0.767}Fe_{0.233}O_{2.87}$ the Mn/Fe–O bond lengths range from 1.94 to 2.14 Å, whereas the Fe–O bond lengths in 10H-$BaFeO_{2.8-y}$[9,10] range from 1.94 to 1.859 Å; both are in octahedral coordination.

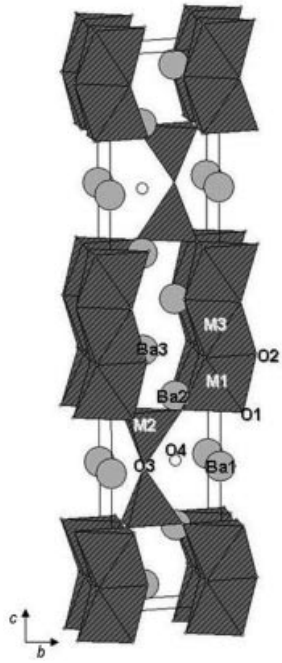

Figure 7. Structural model corresponding to $BaMn_{0.4}Fe_{0.6}O_{2.73}$.

The $Fe2O_4$ tetrahedra are quite distorted with three long Fe2–O1 bonds (1.860 Å) and one short Fe2–O3 bond (1.71 Å). These values are close to those observed in the 10H-$BaFeO_{2.8-y}$[9,10] (1.83 and 1.76 Å, respectively). Finally, as in $BaFeO_{2.8-y}$, the long Fe2–O4 distance obtained (3.672 Å) is not within the bonding distance of the M2 cation.

As we have already mentioned, from the XRD data we are unable to discern between the two metals; however, we can propose a tentative cationic distribution over the different sites. In this sense, it is well known that the presence of Mn stabilizes strings of various face-sharing octahedra in such a way that Mn^{IV} shows a strong preference for occupying the central one of these units. Therefore, we can assume that Mn should be located mainly in the center of the trimers. This fact is well in accordance with the high symmetry of this M3 site. The units of tetrahedra sharing corners involve only Fe (probably in the III oxidation state); therefore, according to the Mn/Fe experimental cationic ratio of 0.4:0.6, Mn/Fe should occupy the outer octahedra of the trimer units in a ratio close to 50:50. If Mn is stabilized as Mn^{IV}, the oxidation state of the Fe remaining in this polyhedron should be close to 3.3; this fact indicates the presence of Fe^{IV} in this polyhedron, whose high-spin configuration should be stabilized by the large distortion of the M1 site. The large contrast between the scattering lengths of Mn and Fe makes neutron scattering a particularly sensitive tool in this case. Therefore, in order to confirm these crystallochemical considerations, a neutron diffraction study is in progress.

We would like to emphasize that, from single-crystal XRD analysis, an orthorhombic deformation is found in 10H-$BaFeO_{2.80}$ (*Cmcm* space group).[10] This lower symmetry seems to be caused by a displacement of barium and oxygen atoms in the BaO_2 layers from hexagonal special positions, changing the symmetry from hexagonal to orthorhombic. We have also performed the refinement of the 10H-$BaMn_{0.4}Fe_{0.6}O_{2.73}$ structure by using the orthorhombic description reported for the 10H-$BaFeO_{2.8}$ polytype. However, even though a similar displacement of the barium into the BaO_2 layers seems occur, we are unable to draw any meaningful conclusion in relation to this symmetry change, since it is not possible to obtain accurate atomic positions of the oxygen atoms from powder X-ray diffraction analysis.

Magnetic Properties

The magnetic properties of 10H-$BaMn_{0.4}Fe_{0.6}O_{2.73}$ have also been explored. Figure 8 shows the temperature dependence of the magnetic susceptibility as measured in a field of 1000 Oe. A very slight divergence between the zero-field-cooled (ZFC) and field-cooled (FC) data opens up below 150 K. Besides, low values, close to 2.4×10^{-3} emu/mol, and weak temperature dependence of the magnetic susceptibility are observed above 100 K. These features suggest the presence of strong interactions between magnetic cations in this temperature range; the negative temperature intercept shown in the inverse magnetic susceptibility plot can indicate that these interactions are antiferromagnetic. Analogous behavior has been evidenced in other Mn polytypes, as in 4H-$SrMnO_{3-x}$[17] where only short-range antiferromagnetic coupling between the Mn^{4+} cations in the Mn_2O_9 face-sharing octahedra is detected. In a similar way, it can be considered that short-range antiferromagnetic coupling takes place between the Mn^{4+} cations in the Mn_3O_9 structural units in $BaMn_{0.4}Fe_{0.6}O_{2.73}$. However, long-range interactions do not occur, since it is no indication of 3D magnetic order in the susceptibility data at low temperatures. Because of these short-range interactions, we cannot obtain the oxidation state of Mn/Fe cations from the magnetic susceptibility curve. Nevertheless, according to the anionic stoichiometry of the sample and on the basis of crystallochemical considerations, the following formulation $Ba[(Mn_{0.2}^{IV})(Fe_{0.14}^{III}Fe_{0.06}^{IV})]_{Oh1}[Mn_{0.2}^{IV}]_{Oh3}[Fe_{0.4}^{III}]_{td}O_{2.73}$ can be proposed for the investigated sample.

Experimental Section

The black polycrystalline sample of $BaMn_{0.4}Fe_{0.6}O_{3-y}$ was prepared from a well-ground stoichiometric mixture of $BaCO_3$ (Aldrich, 99.98%), $MnCO_3$ (Aldrich, 99%), and Fe_2O_3 (Aldrich, 99.98%). The mixture was heated in an Al_2O_3 crucible at 900 °C in air for 48 h. Then, the sample was treated at 1200 °C for one

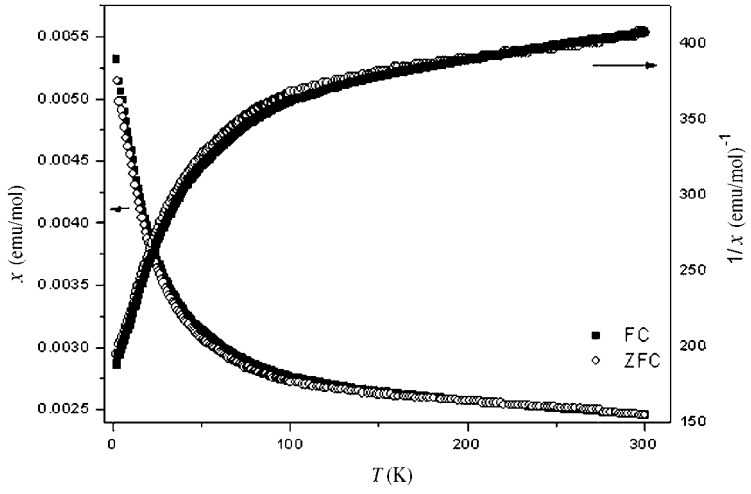

Figure 8. Temperature dependence of the magnetic susceptibility under an applied magnetic field of 1000 Oe.

day and then quenched to room temperature. This process was repeated four times with intermediate grinding in order to ensure homogeneity.

The average cationic composition was determined by Inductively Coupled Plasma (ICP) analysis, whereas the local composition was analyzed by EDS with an INCA analyzer system attached to a JEOL 3000 FEG electron microscope. The overall oxygen content was determined by thermogravimetric analysis with a thermobalance based on a CAHN D-200 electrobalance, which allows the determination of variations of the oxygen content within $\pm 1 \times 10^{-3}$ on a sample of about 100 mg when working under an atmosphere of 500 mbar gas.

Powder XRD patterns were collected by using Cu-K_α radiation (λ = 1.5418 Å) at room temperature with a PHILIPS X′PERT PRO MPD diffractometer equipped with a germanium monochromator. Diffraction data were analyzed by the Rietveld method[18] using the Fullprof program.[19]

SAED and HREM were performed with a JEOL 3000 FEG electron microscope fitted with a double-tilting goniometer stage ($\pm$ 22°, $\pm$ 22°). Simulated HREM images were calculated by the multislice method with the MacTempas software package.

Acknowledgments

Financial support by MEC (Spain) through research project MAT2004–01248 is acknowledged.

[1] A. Hardy, *Acta Crystallogr.* **1962**, *15*, 179–181.
[2] T. Negas, R. S. Roth, *J. Solid State Chem.* **1971**, *3*, 323–339.
[3] M. Parras, J. M. González-Calbet, J. Alonso, M. Vallet-Regí, *J. Solid State Chem.* **1994**, *113*, 78–87.
[4] J. M. González-Calbet, M. Parras, J. Alonso, M. Vallet-Regí, *J. Solid State Chem.* **1994**, *111*, 202–207.
[5] M. Parras, J. Alonso, J. M. González-Calbet, M. Vallet-Regí, *J. Solid State Chem.* **1995**, *117*, 21–29.
[6] A. J. Jacobson, *Acta Crystallogr., Sect. B* **1976**, *32*, 1087–1090.
[7] J. M. González-Calbet, M. Parras, M. Vallet-Regí, J. C. Grenier, *J. Solid State Chem.* **1990**, *86*, 149–159.
[8] Z. Zou, S. Hovmoller, M. Parras, J. M. González-Calbet, M. Vallet-Regí, J. C. Grenier, *Acta Crystallogr. A* **1993**, *49*, 27–35.
[9] M. I. Gómez, G. Lucotti, J. A. de Moran, P. J. Aymonino, S. Pagola, P. Stephens, R. E. Carbonio, *J. Solid State Chem.* **2001**, *160*, 17–24.
[10] J. D. Delattre, A. m. Stacy, T. Siegrist, *J. Solid State Chem.* **2004**, *177*, 928–935.
[11] I. Muro, M. Isausti, L. Lezama, T. Rojo, *J. Solid State Chem.* **2005**, *178*, 1712–1719.
[12] R. D. Shannon, *Acta Crystallogr., Sect. A* **1976**, *32*, 751–767.
[13] V. Caignaert, M. Hervieu, B. Domengès, N. Nguyen, J. Pannetier, B. Raveau, *J. Solid State Chem.* **1988**, *73*, 107–117.
[14] P. D. Battle, C. M. Davison, T. C. Gibbs, J. F. Vente, *J. Mater. Chem.* **1996**, *6*, 1187–1190.
[15] E. J. Cussen, P. D. Battle, *Chem. Mater.* **2000**, *12*, 831–838.
[16] N. A. Jordan, P. D. Battle, *J. Mater. Chem.* **2003**, *9*, 2220–2226.
[17] P. D. Battle, T. C. Giba, C. W. Jones, *J. Solid State Chem.* **1988**, *74*, 60–66.
[18] H. M. Rietveld, *J. Appl. Crystallogr.* **1969**, *2*, 65–71.
[19] J. Rodríguez-Carvajal, *Physica B* **1993**, *192*, 55–69.

Received: December 11, 2006
Published Online: April 10, 2007

